doi:10.1093/brain/awn105 *Brain* (2008), **131**, 1722–1735

Mitochondrial defects in acute multiple sclerosis lesions

Don Mahad,[1] Iryna Ziabreva,[1] Hans Lassmann[2] and Douglas Turnbull[1]

[1]The Mitochondrial Research Group, University of Newcastle upon Tyne, UK and [2]Centre for Brain Research, Medical University of Vienna, Austria

Correspondence to: Prof. Dr Hans Lassmann, Center for Brain Research, Medical University of Vienna, Spitalgasse 4, A-1090 Wien Austria
E-mail: hans.lassmann@meduniwien.ac.at

Multiple sclerosis is a chronic inflammatory disease, which leads to focal plaques of demyelination and tissue injury in the CNS. The structural and immunopathological patterns of demyelination suggest that different immune mechanisms may be involved in tissue damage. In a subtype of lesions, which are mainly found in patients with acute fulminant multiple sclerosis with Balo's type concentric sclerosis and in a subset of early relapsing remitting multiple sclerosis, the initial myelin changes closely resemble those seen in white matter stroke (WMS), suggesting a hypoxia-like tissue injury. Since mitochondrial injury may be involved in the pathogenesis of such lesions, we analysed a number of mitochondrial respiratory chain proteins in active lesions from acute multiple sclerosis and from WMS using immunohistochemistry. Functionally important defects of mitochondrial respiratory chain complex IV [cytochrome c oxidase (COX)] including its catalytic component (COX-I) are present in Pattern III but not in Pattern II multiple sclerosis lesions. The lack of immunohistochemically detected COX-I is apparent in oligodendrocytes, hypertrophied astrocytes and axons, but not in microglia. The profile of immunohistochemically detected mitochondrial respiratory chain complex subunits differs between multiple sclerosis and WMS. The findings suggest that hypoxia-like tissue injury in Pattern III multiple sclerosis lesions may be due to mitochondrial impairment.

Keywords: multiple sclerosis; Pattern III lesion; mitochondria; cytochrome c oxidase

Abbreviations: CNPase = cyclic nucleotide phosphodiesterase; COX = cytochrome c oxidase; LFB = Luxol fast blue; MAG = myelin associated glycoprotein; MBP = myelin basic protein; mtDNA = mitochondrial DNA; NO = nitric oxide; NWM = normal white matter; PLP = proteolipid protein; WMS = white matter stroke

Received February 22, 2008. Revised April 25, 2008. Accepted May 1, 2008. Advance Access publication May 30, 2008

Introduction

Multiple sclerosis is an inflammatory demyelinating disease of the central nervous system with axonal degeneration and astrogliosis (Frohman *et al.*, 2006). The loss of myelin in multiple sclerosis may be the result of direct damage to myelin through immune mediated processes and/or dysfunction of oligodendrocytes (Lassmann *et al.*, 2001; Barnett and Prineas, 2004). A particular subtype of active multiple sclerosis lesions (Pattern III, Lucchinetti *et al* 2000), which are mainly found in patients with acute fulminant multiple sclerosis with Balo's type concentric sclerosis and in a subset of early relapsing remitting multiple sclerosis, has been defined by the selective early loss of myelin associated glycoprotein (MAG) and cyclic nucleotide phosphodiesterase (CNPase) together with apoptotic cell death of oligodendrocytes (Itoyama *et al.*, 1980; Lucchinetti *et al.*, 2000; Barnett and Prineas, 2004; Stadelmann *et al.*, 2005). Indirect evidence suggests that hypoxia-like tissue injury may play a role in their pathogenesis. A comparable loss of MAG and CNPase together with oligodendrocyte apoptosis is also seen in initial lesions in white matter stroke (WMS) and hypoxia inducible factor-1α, a transcription factor induced in hypoxic condition, is expressed in such multiple sclerosis and WMS lesions (Aboul-Enein *et al.*, 2003; Stadelmann *et al.*, 2005). Profound microglia and macrophage activation with expression of inducible nitric oxide synthase (i-NOS) and myeloperoxidase is another characteristic feature of such multiple sclerosis lesions (Stadelmann *et al.*, 2005; Marik *et al.*, 2007). Reactive oxygen species and nitric oxide (NO), produced by these enzymes, may impair mitochondrial function (Bolanos *et al.*, 1997) and thus may link

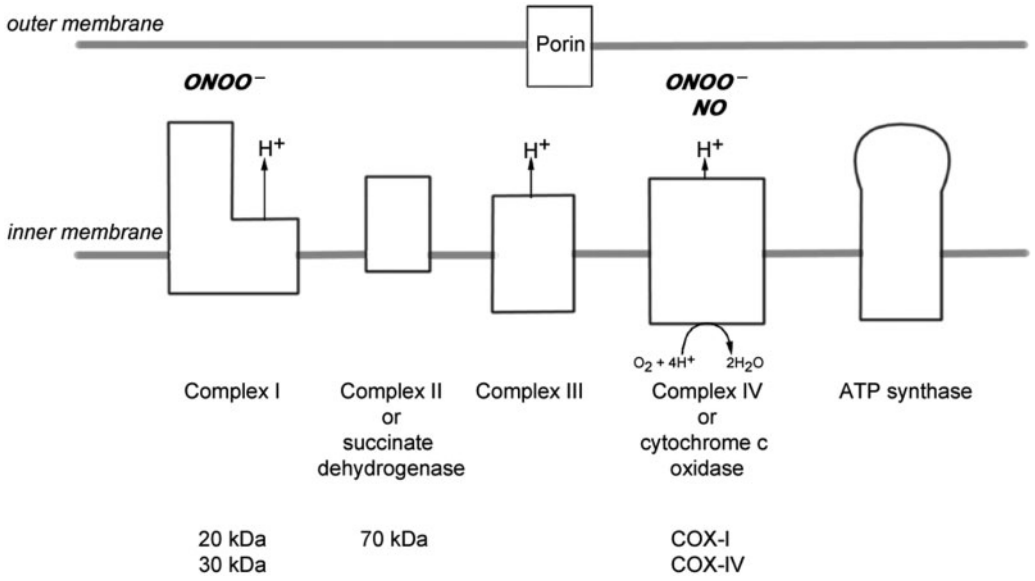

Fig. 1 The mitochondrial respiratory chain. The mitochondrial respiratory chain consists of four complexes (complexes I–IV) and complex V, which is directly involved in ATP synthesis. The complexes are made up of multiple subunits encoded by nuclear DNA and mtDNA, except complex II which is entirely encoded by nuclear DNA. We investigated two subunits of complex I (20 and 30 kDa), one of complex II (70 kDa) and two of complex IV (subunits I and IV of complex IV or COX-I and COX-IV, respectively) in brain tissue. Porin, a voltage gated anion channel located in the outer mitochondrial membrane, was used as a mitochondrial marker. The activity of succinate dehydrogenase (complex II) and COX (complex IV) can be determined at the single cell level using an enzyme histochemical assay (COX/succinate dehydrogenase histochemistry). NO inhibits complex IV activity by competing with oxygen for the oxygen binding sites, of which three out of the four are located in COX-I. Both complexes I and IV are susceptible to peroxynitrite ($ONOO^-$) mediated damage.

microglial activation in such lesions with a hypoxia-like tissue injury.

Mitochondria contain the respiratory chain where energy in the form of ATP is most efficiently produced (DiMauro and Schon, 2003). Mitochondria also play an important role in apoptosis and calcium homeostasis (Rizzuto and Pozzan, 2006; Kalman *et al.*, 2007). The mitochondrial respiratory chain is located in the inner mitochondrial membrane and consists of four complexes (complexes I–IV, Fig. 1) whilst complex V is directly involved in ATP synthesis (DiMauro and Schon, 2003). The complexes of the mitochondrial respiratory chain are made up of multiple subunits and all but complex II (which is entirely encoded by nuclear DNA) contain proteins encoded by nuclear and mitochondrial DNA (mtDNA) (Taylor and Turnbull, 2005). The final respiratory chain complex [complex IV or cytochrome c oxidase (COX)] is the site at which over 90% of oxygen is consumed (DiMauro and Schon, 2003). This complex is also involved in proton pumping, essential for ATP synthesis (DiMauro and Schon, 2003). NO competitively inhibits the binding of oxygen to complex IV (Brown and Cooper, 1994; Cleeter *et al.*, 1994). NO, when overexpressed, may irreversibly impair the activity of mitochondrial respiratory chain complexes I and IV via perxoynitrite (Clementi *et al.*, 1998; Smith and Lassmann, 2002; Zhang *et al.*, 2005). In pathological states, histotoxic hypoxia may be induced by the inability to use available oxygen, when complex IV is blocked by persistently increased NO levels (Moncada and Erusalimsky, 2002). Three of the four oxygen binding sites [heme (a and a3) and copper (CuB) cofactors] are located in subunit-I of complex IV (COX-I), which is the vital component of the catalytic core (Taanman and Williams, 2001). COX-I, encoded by mtDNA, is highly conserved in eukaryotic cells (Taanman and Williams, 2001; Taylor and Turnbull, 2005). The loss of COX-I renders complex IV inactive as reported in patients with mitochondrial disease due to pathogenic mutations of COX-I gene and prevents utilization of oxygen (Clementi *et al.*, 1998; Bruno *et al.*, 1999; Kollberg *et al.*, 2005).

Based on the evidence that NO impairs mitochondrial respiratory chain complexes, HIF-1α regulates the composition of subunits of complex IV and NO and HIF-1α are present in Pattern III multiple sclerosis lesions, we hypothesized that defects in mitochondrial respiratory chain complexes may be involved in hypoxia-like tissue damage in Pattern III lesions of multiple sclerosis patients.

Materials and Methods

Autopsy tissue

Paraffin embedded brain tissue from acute multiple sclerosis cases is part of the well-characterized archival material used to identify the four patterns of acute multiple sclerosis lesions (MS1–MS9, Table 1) (Lucchinetti *et al.*, 2000). Tissue from WMS cases (WMS1–WMS6, Table 1) containing lesions with active demyelination was provided by the University of Vienna (Aboul-Enein *et al.*, 2003). Control tissue (CON1–CON8, Table 1) was provided by the UK multiple sclerosis tissue resource, London. Although the exact post-mortem delay for the acute multiple sclerosis cases

Table 1 Details of autopsy cases

Case No.	Age (years)/Sex	Diagnosis	No. of blocks	No. of lesions	Duration of disease
MS1	45/F	Acute multiple sclerosis (Pattern III)	2[a]	3	1 week
MS2	45/F	Acute multiple sclerosis (Pattern III)	1	1	2 months
MS3	35/M	Acute multiple sclerosis (Pattern III)	2[a]	3	1.5 months
MS4	44/F	Acute multiple sclerosis (Pattern III)	2[a]	3	2 weeks
MS5	40/F	Acute multiple sclerosis (Pattern III)	2	2	120 months
MS6	46/F	Acute multiple sclerosis (Pattern II)	2	2	3 months
MS7	51/F	Acute multiple sclerosis (Pattern II)	2	3	5 months
MS8	52/M	Acute multiple sclerosis (Pattern II)	2	3	1.5 months
MS9	20/F	Acute multiple sclerosis (Pattern II)	1	1	4 years
WMS1	51/F	WMS	1	1	2 weeks
WMS2	66/M	WMS	1	2	1.5 months
WMS3	68/M	WMS	1	2	1 week
WMS4	85/F	WMS	1	2	1.5 months
WMS5	90/F	WMS	1	2	0.6 weeks
WMS6	85/F	WMS	1	1	1.1 weeks
CON1	85/M	NND	2	NA	NA
CON2	89/M	NND	2	NA	NA
CON3	57/M	NND	2	NA	NA
CON4	95/F	NND	2	NA	NA
CON5	67/F	NND	2	NA	NA
CON6	64/F	NND	2	NA	NA
CON7	88/M	NND	2	NA	NA
CON8	76/F	NND	2	NA	NA

CON = control; NA = not applicable; NND = non-neurological disease (carcinomatosis originating from bowel or prostate).
[a]The large sections measured ~4.5 × 3 cms.

Table 2 Details of antibodies used for immunohistochemistry

Antigen	Encoding DNA	Antibody type	Source
MBP (SMI 94)	–	mouse IgG_1	Sternberger
PLP	–	mouse IgG	Serotec
MAG (D7EI0)	–	mouse IgG	(Dobersen et al., 1985)
CNPase	–	mouse IgG_1	Sternberger
HLA-DP, DQ and DR	–	mouse IgG_1	Dako
CDI63	–	mouse IgG_1	Novocastra
Glial fibrillary acidic protein	–	rabbit polyclonal	Dako
Phosphorylated NF (SMI 31)	–	mouse IgG_1	Sternberger
Non-phosphorylated NF (SMI32)	–	mouse IgG_1	Sternberger
Porin	Nuclear	mouse IgG_{2b}	Invitrogen
Complex I-20 kDa (MTND6)*	Mitochondrial	mouse IgG_1	Invitrogen
Complex I-30 kDa (NDUFS3)*	Nuclear	mouse IgG_1	Invitrogen
Complex II 70 kDa (SDHA)*	Nuclear	mouse IgG_{2a}	Invitrogen
Complex IV subunit-I or COX-I (MTCOI)*	Mitochondrial	mouse IgG_{2a}	Invitrogen
Complex IV subunit-IV or COX-IV (COX4)*	Nuclear	mouse IgG_{2a}	Invitrogen

*Gene number.

are unknown, the tissue is well preserved with respect to detection of mRNA by *in situ* hybridization as well as protein epitopes by immunohistochemistry. For fixed control tissue, the range for post-mortem time is 4–63 h (median = 18). The cause of death for all multiple sclerosis cases and controls (Table 1) was either cardiorespiratory failure/arrest or pneumonia. The control cases had underlying carcinomatosis originating from bowel or prostate. For validation of immunoreactivity of monoclonal antibodies against a number of mitochondrial respiratory chain complex subunits in fixed brain tissue, both paraffin embedded and frozen hippocampal sections were used from a case with multiple mtDNA deletions (Taylor and Turnbull, 2005). The Newcastle and North Tyneside Local Research Ethics Committee approved the study (205/Q0906/182).

Immunohistochemistry

Following rehydration of fixed and paraffin embedded sections (5 µm thickness) antigen retrieval was performed using EDTA buffer pH 8.0. The endogenous peroxidase activity was blocked using 3% hydrogen peroxide for 30 min and non-specific antibody binding was prevented by blocking sections in 1% normal goat serum (Sigma) for 30 min prior to incubation with the primary antibody (Table 2). Both mtDNA and nuclear DNA encoded

subunits were included for the immunohistochemical detection (Rahman *et al*., 2000; Taylor and Turnbull, 2005). The secondary antibody (goat anti-mouse or goat anti-rabbit, Vector), avidin-biotin amplification system with peroxidase (Vector) and diamino benzidine tetrahydrochloride (DAB, Sigma) were used according to manufactures protocols. The sections were counter stained with hematoxylin prior to dehydration and mounting. Serial sections from each block were used for staining with antibodies against mitochondrial respiratory chain subunits and porin, a voltage-dependant anion channel expressed on the outer mitochondrial membrane (Table 2). For co-staining using chromogens (DAB and Vector SG) one anti-mitochondrial respiratory chain subunit antibody was developed with DAB (brown) and then the sections were re-blocked and incubated with anti-glial fibrillarry acidic protein antibody which was detected using HRP conjugated anti-rabbit secondary antibody (DAKO) and Vector SG (grey). The appropriate control experiments were performed to exclude cross reactivity of secondary antibodies.

Immunofluorescent histochemistry

Dual immunofluorescence was utilized for cellular localization of mitochondrial respiratory chain subunits. The paraffin embedded tissue sections were prepared as for immunohistochemistry without hydrogen peroxide. The pairs of primary antibodies were co-incubated for 90 min at room temperature followed by two subtype specific secondary antibodies (Jackson immunoresearch), one rhodamine conjugated and other biotinylated. The biotinylated secondary antibody was amplified using streptavidin fluoroisothiocyanate (Alexis). The sections were mounted using Vectashield with DAPI (Vector). Lack of cross reactivity and non-specific binding of secondary antibodies was determined using appropriate controls.

Histochemistry

For detection of complex IV activity within individual cells in the case with primary mitochondrial disease, frozen hippocampal sections (8 µm) were air dried for 60 min at room temperature prior to incubation in COX medium (100 µM cytochrome c, 4 mM diaminobenzidine tetrahydro-chloride and 20 µg/ml catalase in 0.2 M phosphate buffer, pH 7.0) at 37°C for 50 min (Clark *et al*., 1997). To detect mitochondrial elements that lack complex IV activity, the activity of complex II (unaffected by the mtDNA deletions) was determined by incubating in succinate dehydrogenase medium (130 mM sodium succinate, 200 µM phenazine methosulphate, 1 mM sodium azide, 1.5 mM nitroblue tetrazolium in 0.2 M phosphate buffer, pH 7.0) at 37°C for 40 min once the incubation in COX medium for 50 min and the subsequent washing steps were completed. Following histochemistry, the sections were dehydrated in 70, 90 and 100% ethanol followed by Histoclear (National Diagnostics, Atlanta, Georgia, USA) and mounted in Glycerol (Citifluor).

Lesion classification

The Pattern III lesions in the early active (EA) stage ($n = 12$), including Balo's type, were identified based on the preferential loss of MAG or CNPase and the absence of immunoglobulins and complement deposition, as previously described (Lucchinetti *et al*., 2000). In contrast, Pattern II lesions, similarly staged by the presence of early myelin degradation products in macrophages ($n = 9$), show a comparable loss of MAG and other myelin components [myelin basic protein (MBP), proteolipid protein (PLP) and myelin oligodendrocyte glycoprotein]. The EA regions of WMS lesions ($n = 10$) showed preferential loss of MAG and CNPase as in Pattern III lesions. The late active (LA) regions of all lesion types are demyelinated and contain phagocytic macrophages with only the major myelin degradation products (MBP, PLP and myelin oligodendrocyte glycoprotein). All lesion types show inflammatory activity as shown by HLA staining. No lesions were present in control tissue. The two stages of demyelination (EA and LA) were present in all Pattern III, 8 of the 9 Pattern II and 9 of the 10 WMS lesions. One Pattern II lesion and one WMS lesion contained only a LA and EA stage, respectively. The regions of 'normal' white matter (NWM), without macroscopic or histological evidence of demyelination, were identified as internal controls for Pattern III ($n = 12$), Pattern II ($n = 9$) and WMS ($n = 10$) lesions.

Confocal laser fluorescence microscopy

The sections double labelled for mitochondrial proteins and neurofilaments (SMI31 and SMI32) or CNPase using immunofluorescence were analysed on a Leica laser scanning microscope (Heidelberg, Germany). Individual optical sections with 1 µm thickness were taken through the tissue sections. The minimum number of optical sections was combined to track axons in Pattern III lesions. fluoroisothiocyanate and TRIC channels were imaged sequentially and the optimal number of images stacked to ensure that the yellow elements are a result of co-localisation rather than superimposition of non-axonal porin (fluoroisothiocyanate) elements. The offset and gain were kept constant during imaging of all sections. A single x–z optical section was taken through axons.

Quantification of mitochondrial respiratory chain complex subunit immunoreactivity in fixed brain tissue

Due to the ubiquitous nature of mitochondrial immunoreactivity in the brain, the immunoreactive elements were captured using a 100× oil lens (Axioplan, Zeiss) and the well demarcated punctate elements were manually counted in two 100× fields (6044 µm^2/field) for each lesion stage and NWM of every acute multiple sclerosis and WMS case. We also counted the immunoreactive elements within individual hippocampal cells from the case with mtDNA deletions. The assessors were blinded to tissue type and lesion stage. In order to correct for loss of tissue and/or mitochondria, the immunoreactivity of mitochondrial respiratory chain complex subunits is calculated as a percentage of porin immunoreactivity within each region in serial sections. The difficulty in identifying individual immunoreactive elements within cell bodies of glia limited the manual quantitation of immunoreactivity within hypertrophied astrocytes and activated microglia, which were excluded from this analysis. As the second method of analysis, the optical density of grey scale 100× images with identical exposure times were measured using densitometry (Zeiss Axiovision), which included immunoreactive elements within glia.

Statistical analysis

Parametric tests (ANOVA) and SPSS version 14 were used for statistical analysis of immunoreactivity in multiple sclerosis, WMS

and control white matter cases as well as the mitochondrial case. The immunoreactivity within lesion stages were compared with the corresponding NWM in multiple sclerosis and WMS cases using the posttest (Newman-Keuls), when ANOVA test indicated a P-value of <0.05.

Results

Since hypoxia-like tissue injury, described in a subset of multiple sclerosis lesions (Pattern III, Lucchinetti *et* al., 2000), may be caused by mitochondrial dysfunction we analysed the expression patterns of mitochondrial proteins in these lesions in comparison to that in other multiple sclerosis lesions (Pattern II) and control brain white matter by quantitative immunohistochemistry (Lucchinetti *et al.*, 2000). We then correlated our findings in multiple sclerosis with those seen in lesions of acute WMS and mitochondrial encephalopathy.

Pattern III multiple sclerosis lesions show alterations in the expression of mitochondrial proteins, mainly affecting COX-I and COX-IV

Pattern III lesions in multiple sclerosis are inflammatory demyelinating lesions with profound microglial activation (Fig. 2a and b). In the EA stage, they are characterized by reduced myelin density in Luxol fast blue (LFB) stained sections (Fig. 2a) and a prominent loss of MAG (Fig. 2c) and CNPase, while other myelin proteins remain preserved (Fig. 2d). In more advanced lesions, called LA lesions, myelin is completely lost (Fig. 2a, c and d). Some of the lesions may show concentric rims of demyelinated and myelinated tissue (Fig. 2a, c and d). Staining for mitochondrial proteins revealed a profound loss of COX-I (Fig. 2e and g) and COX-IV of complex IV (Fig. 2i) in EA and LA lesion areas, while a general reduction of mitochondrial density, visualized also by reduction of porin immunoreactivity, was mainly seen in LA lesions where vacuolation of tissue is particularly apparent.

This general impression was confirmed by two independent quantitative methods. The analysis of optical density of affected tissue revealed significant reduction of mitochondrial immunoreactive signal for COX-I in both EA ($P<0.01$) and LA lesional stages ($P<0.001$) in comparison to that in NWM. Counting individual immunoreactive mitochondrial profiles revealed significant reduction of COX-I reactive elements in the EA stage (Table 3). In the LA stage, the number of immunoreactive mitochondria was reduced with all markers used, the most profound reduction was seen for COX-I and COX-IV (Table 3). When the number of COX-I reactive elements was corrected for porin in serial section, the percentage of porin stained mitochondria, which expressed COX-I was reduced to 69 in EA and 43 in LA stages. A profound reduction of immunoreactive mitochondria was also seen for COX-IV in the LA stage (Table 3).

The defect in the catalytic subunit of complex IV (COX-I) in Pattern III multiple sclerosis lesions involves oligodendrocytes, axons and astrocytes, but not macrophages and microglia

In the next step we analysed mitochondrial immunoreactivity in different cell types within active multiple sclerosis lesions by double labelling immunohistochemistry and confocal laser microscopy. The absence or massive decrease of COX-I reactivity was seen in oligodendrocytes (Fig. 3a), axons (Fig. 3c) as well as in a subpopulation (~50%) of glial fibrillary acidic protein positive astrocytes (Fig. 3e), despite the abundance of porin reactive mitochondria in the same cellular sites (Fig. 3b, d and f).

The mitochondria located within activated microglia in EA and LA stages of Pattern III multiple sclerosis lesions retain COX-I immunoreactivity despite the diffuse reduction in COX-I immunoreactivity involving other cell types in the same regions (Fig. 3g–i).

No cellular mitochondrial defects are detectable in Pattern II multiple sclerosis lesions

As in Pattern III, Pattern II multiple sclerosis lesions develop on the background of inflammation with activation of complement (Marik *et al.*, 2007). In EA stages perivenous sheaths of demyelination are seen, which are separated by areas of partly preserved myelin with abundant macrophages, containing early myelin degradation products (Fig. 4a and b). In contrast to Pattern III multiple sclerosis lesions, there is no preferential loss of MAG or CNPase in comparison to other myelin proteins (Fig. 4c and d). At higher magnification, the tissue in EA and LA stages appears vacuolated, due to profound oedema, which extends into the adjacent NWM. A general reduction in the density of mitochondrial profiles, seen in quantitative analysis (Table 3), reflects the absence of mitochondria in oedematous vacuoles (Fig. 4e and f). Within the cellular profiles, however, mitochondrial density is not reduced in comparison to that seen in the NWM of controls. We did not find significant changes in the expression of different mitochondrial proteins between NWM of controls and Pattern II multiple sclerosis lesions, when the expression is corrected for porin containing elements (Table 3).

Widespread defects of mitochondrial respiratory chain complexes in WMS lesions

The transcription of mtDNA and nuclear DNA encoded subunits of the mitochondrial respiratory chain complexes are modulated by hypoxia (Vijayasarathy *et al.*, 2003; Piruat and Lopez-Barneo, 2005; Fukuda *et al.*, 2007).

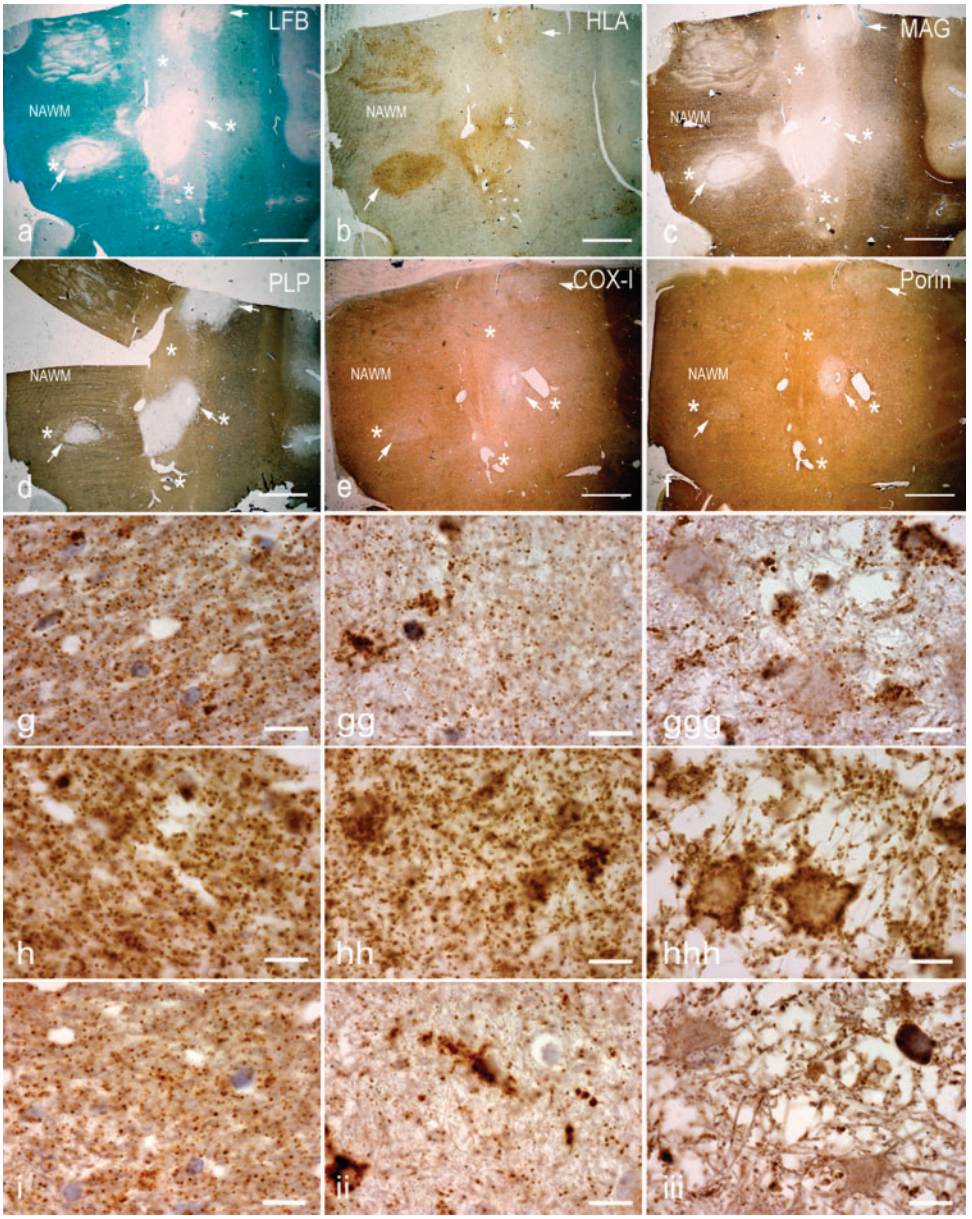

Fig. 2 Pattern III multiple sclerosis lesions. (a–d) The brain sections containing Pattern III and Balo's type (with concentric rings of preserved myelin) active multiple sclerosis lesions are stained for LFB (a), HLA (b), MAG (c)and PLP (d). There is reduced density of LFB staining (a, asterisks) in the EA stage, whereas LFB staining is absent (a, arrows) in the LA stage of Pattern III lesions compared with NWM. The neuropathological hallmark of Pattern III lesions is the preferential loss of MAG, as indicated here by the loss of MAG immunoreactivity (c, asterisks) and intact PLP immunoreactivity (d, asterisks) in the EA stage. In contrast, MAG and PLP immunoreactivity is lost in the LA stage of Pattern III lesions (c and d, arrows). e and f: In deeper sections from the same block, there is a decrease in complex IV subunit-I (COX-I) immunoreactivity, which is diffuse in the EA stage (e, asterisks) and most prominent in the LA stage (e, arrows) compared with NWM. The porin immunoreactivity in the EA stage (f, asterisks) of Pattern III lesions is similar to the NWM. However, there is a decrease in porin immunoreactivity in the LA stage (f, arrows). Interestingly, COX-I immunoreactivity is preserved in the concentric rings of the Balo's type multiple sclerosis lesion (e). g–i: Higher magnification images show the punctate COX-I (g), porin (h) and COX-IV (i) immunoreactive elements, typical of mitochondrial staining, in the NWM (left column), EA stage (middle column) and LA stage (right column). There is a global reduction in the number of COX-I immunoreactive elements in the EA (gg) and LA (ggg) stages of Pattern III lesions compared with NWM (g). There are ramified cells consistent with microglia containing dense COX-I immunoreactivity in Pattern III lesions (gg–ggg). The number of porin immunoreactive elements appears reduced in LA (hhh), where there is tissue vacuolation, but not EA (hh) stage compared with NWM (h). The cells with enlarged cytoplasm (consistent with hypertrophied astrocytes) contain a peripheral rim of dense porin (hhh) but not COX-I (ggg) immunoreactivity, and clearly illustrate the disproportionate loss of COX-I compared with porin immunoreactivity in Pattern III lesions. The number of COX-IV immunoreactive elements is also decreased in Pattern III lesions (ii and iii) compared with NWM (i). Scale bars = 8 mm (a–f) and 10 μm (g–i).

Table 3 Quantitation of immunoreactive elements of mitochondrial respiratory chain subunits and porin in Patterns II and III multiple sclerosis lesions and control white matter

Antigen mean ± SD (No. of lesions)	Porin	COX-I (mtDNA)	COX-IV (nuclear)	Complex I 20 kDa or ND6 (mtDNA)	Complex I 30 kDa (nuclear)	Complex II 70 kDa (nuclear)
CON WM	228.8 ± 23.3	207.2 ± 16.9	152.4 ± 12.8	141.0 ± 16.5	139.3 ± 17.3	119.5 ± 13.4
± SD	–	94.1 ± 6.8	66.0 ± 8.5	67.4 ± 12.7	60.0 ± 9.8	54.7 ± 9.5
(12)	136.1 ± 4.1	144.5 ± 5.6	151.7 ± 3.9	159.6 ± 5.5	147.6 ± 4.3	160.8 ± 3.7
Pattern III MS	202.1 ± 33.9	185.4 ± 17.5	144.2 ± 27.8	131.4 ± 16.9	115.4 ± 26.9	92.9 ± 12.8
NWM	–	93.1 ± 11.6	70.9 ± 16.5	66.4 ± 11.9	61.7 ± 8.5	43.9 ± 8.8
(12)	135.8 ± 4.1	141.5 ± 3.6	160.5 ± 5.1	157.1 ± 3.8	144.3 ± 3.7	161.7 ± 4.7
Pattern III MS	193.1 ± 26.6	131.0 ± 17.6*	112.4 ± 24.7	141.1 ± 17.8	104.7 ± 18.5	101.4 ± 16.4
EA	–	69.0 ± 7.5†	57.7 ± 9.3	71.1 ± 8.2	53.3 ± 12.7	55 ± 13.7
(9–12)	132.9 ± 4.9	170.4 ± 5.1†	166.4 ± 5.2	160.3 ± 3.2	142.6 ± 3.3	157.8 ± 4.8
Pattern III MS	81.7 ± 22.2*	38.8 ± 13.1*	37.7 ± 9.3†	53.7 ± 22.6	43.3 ± 22.7	49.0 ± 8.9
LA	–	43.3 ± 6.1*	47.4 ± 7.3†	66.7 ± 12.1	54.3 ± 10.0	58 ± 6.4
(10–12)	158.8 ± 4.1*	180.9 ± 5.8*	177.9 ± 4.7†	162.2 ± 4.1	143.4 ± 3.9	155.6 ± 4.7
Pattern II MS	198.6 ± 27.9	179.4 ± 14.7	130.7 ± 25.2	128.7 ± 17.5	111.8 ± 10.0	88.3 ± 9.9
NWM	–	89.4 ± 9.5	68.8 ± 15.2	64.3 ± 9.6	58.1 ± 10.2	38 ± 5.8
(8–9)	135.45 ± 3.3	141.1 ± 3.8	154.7 ± 4.3	157.1 ± 4.2	148.2 ± 5.8	159.5 ± 3.9
Pattern II MS	143.4 ± 19.6†	111.3 ± 8.2	99.5 ± 15.3	92.8 ± 14.7	75.9 ± 9.7	104.6 ± 9.4
EA	–	79.9 ± 8.1	71.9 ± 11.7	66.1 ± 12.6	53.3 ± 9.9	40 ± 7.4
(7–8)	128.9 ± 4.1	144.7 ± 5.7	152.3 ± 3.3	156.9 ± 4.7	146.4 ± 3.9	157.2 ± 4.2
Pattern II MS	138.3 ± 14.8†	118.6 ± 11.5	87.9 ± 12.4	86.9 ± 12.6	77.1 ± 10.2	76.8 ± 9.9
LA	–	82.2 ± 9.5	68.8 ± 9.4	65.6 ± 8.5	54.9 ± 10.4	48 ± 6.2
(8–9)	125.1 ± 4.1	138.8 ± 3.8	150.7 ± 4.2	154.3 ± 4.3	142.6 ± 5.1	155.5 ± 3.8

The values indicated in the first line are the mean and standard deviation of the absolute number of punctate elements per 100x field (6044 μm^2), second line are the mean and standard deviation of the percentages of porin elements containing respiratory chain complex subunit immunoreactivity (in serial sections) and third line are the mean and standard deviation of the densitometric values of whole grey scale 100x images. The densitometric value is inversely related to the intensity of the immunoreactivity. The number of lesions or NWM regions analysed for each stage is indicated within parentheses in column one. The immunoreactivity within lesions was compared with the corresponding NWM in multiple sclerosis and WMS cases (†$P<0.01$ and *$P<0.001$).
CON WM = control white matter. EA = early active stage. LA = late active stage. MS = multiple sclerosis. NWM = normal white matter.

Therefore, we immunohistochemically analysed mitochondrial respiratory chain subunits in WMS lesions (Table 4). Similar to Pattern III multiple sclerosis lesions, the EA stage of WMS lesions is characterized by the loss of MAG and CNPase, while other myelin proteins are preserved (Aboul-Enein *et al.*, 2003). In the LA stage tissue is severely damaged, reflected by global loss of myelin, profound axonal degeneration and astrocytic damage (Fig. 5a–bbb). In contrast to multiple sclerosis Pattern III lesions, all the mtDNA and nuclear DNA encoded mitochondrial proteins, with the exception of complex IV, were reduced in the EA stage (Fig. 5c–hhh, Table 4). When corrected for porin expression a significant decrease of mitochondrial immunoreactivity was seen for COX-I, complex I 20 kDa or ND6, complex I 30 kDa and complex II 70 kDa proteins, but not for COX-IV. In LA lesions, where tissue loss is extensive, we found a general loss of mitochondria (including porin reactive elements) except within phagocytic macrophages (Fig. 5ccc–hhh). These data show, that Pattern III multiple sclerosis as well as WMS lesions are associated with mitochondrial injury, but that the profiles of mitochondrial injury are different.

Reduced mitochondrial respiratory chain complex subunit immunoreactivity is associated with decreased functional complex IV activity in mitochondrial encephalopathy

So far we have shown that the expression of mitochondrial proteins, in particular COX-I and COX-IV, is reduced in oligodendrocytes, axons and astrocytes in Pattern III multiple sclerosis lesions and that this reduction is associated with a hypoxia-like tissue injury. The question thus arises, whether such a decrease in mitochondrial proteins may result in a functional defect of the respiratory chain. This can be analysed in frozen tissue sections at the single cell level using enzyme histochemistry for COX

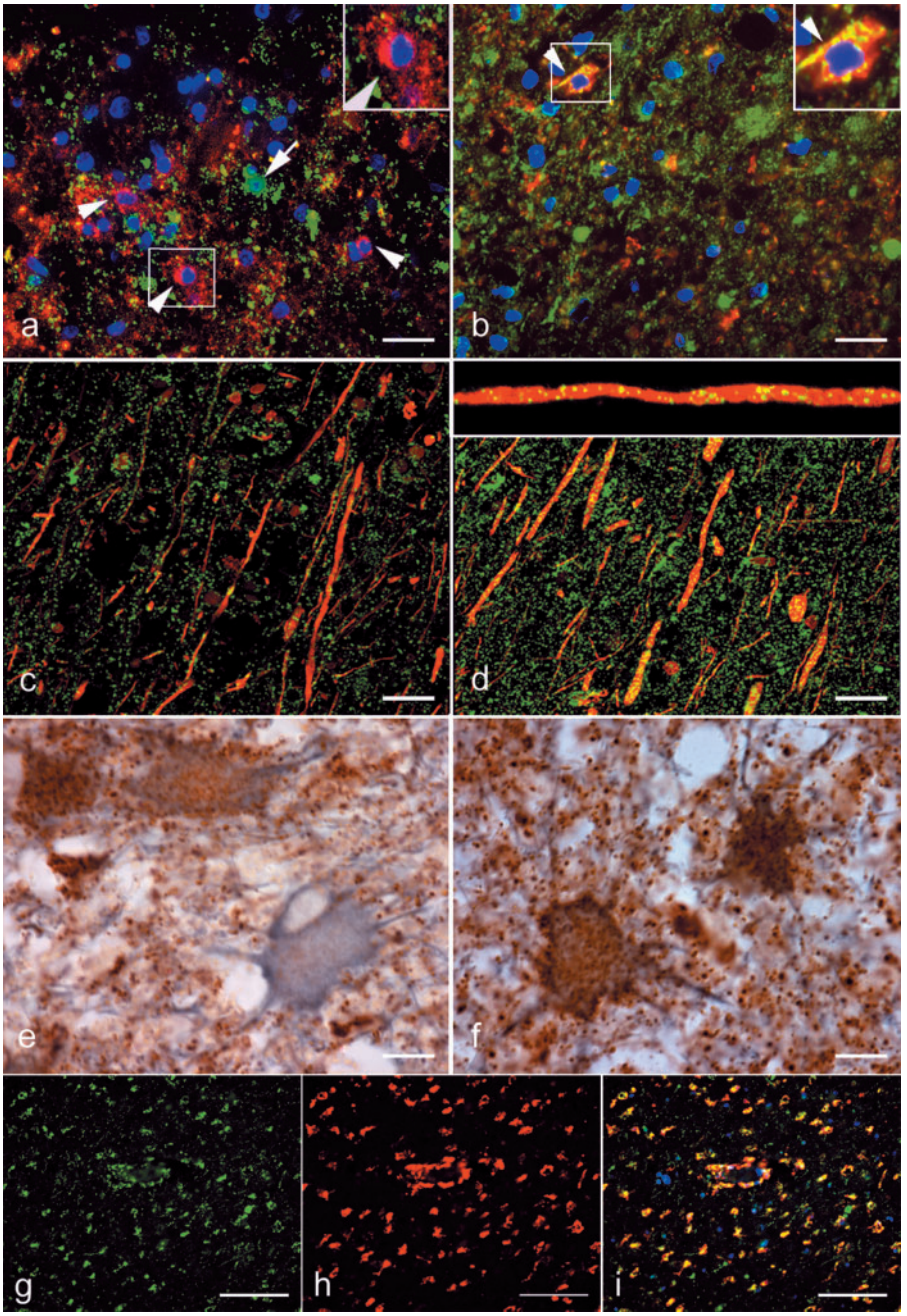

Fig. 3 The oligodendrocytes, axons and hypertrophied astrocytes but not microglia lack COX-I immunoreactivity in Pattern III multiple sclerosis lesions. a–f: The left and right columns of images show COX-I and porin immunoreactivity, respectively. a and b: The double immunofluorescent labelling of COX-I (a, green) and oligodendrocyte marker, CNPase (a, red) identifies oligodendrocytes lacking COX-I immunoreactivity (a, arrowheads and insert) in the EA stage of Pattern III lesions. The cells with COX-I immunoreactivity in the EA stage lack CNPase immunoreactivity (a, arrow). In serial sections, CNPase (red) immunoreactive oligodendrocytes (b, arrowhead and insert) as well as numerous other cells in EA stage contain porin (green) immunoreactive elements. c and d: The double immunofluorescent labelling of COX-I (c, green) and axonal markers [phosphorylated (SMI31) and non-phosphorylated (SMI32) neurofilaments in red] identifies axons with only a small number of COX-I immunoreactive elements (c) in the LA stage of Pattern III lesions. In serial sections, the porin elements (d, green) are more numerous than COX-I elements (c, green) within demyelinated axons in the LA stage of Pattern III lesions. A confocal x–z image (d, insert) confirms the axonal location of the porin immunoreactive elements in the x–y images (d). e and f: The mitochondrial proteins [COX-I (e) and porin (f)] are co-stained with a astrocyte marker, glial fibrillarry acidic protein, using chromogens [DAB (brown) and Vector SG (grey), respectively]. The COX-I immunoreactive elements are absent in a proportion of hypertrophied astrocytes (e) in Pattern III lesions. The hypertrophied astrocytes in serial sections contain abundant porin immunoreactivity (f). g–i: In the LA stage of Pattern III lesions, the activated microglia distributed around the blood vessels and identified by the CD163 (h, red) immunoreactivity contain COX-I immunoreactivity (g and i, green). a–d: Confocal images. Scale bars = 10 μm (a–f) and 50 μm (g–i).

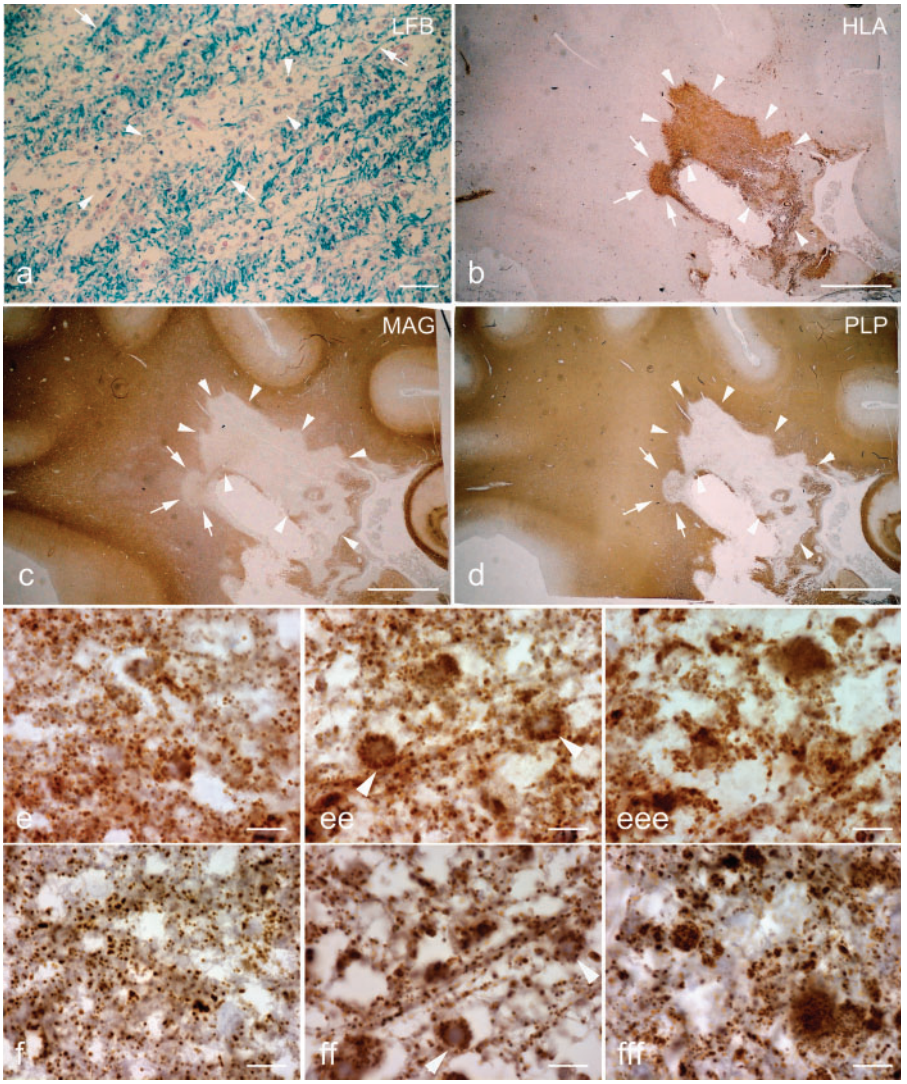

Fig. 4 Pattern II multiple sclerosis lesions. a–d: Sections containing a Pattern II multiple sclerosis lesion are stained for LFB (a), HLA (b), MAG (c) and PLP (d). The EA stage of Pattern II lesions is identified by the perivenous demyelination, which are separated by partly preserved myelin (a, arrows), and abundance of phagocytic macrophages (b) containing myelin debris (a, arrowheads). Both MAG (c) and PLP (d) immunoreactivity are equally lost in the EA and LA stages (c and d, arrows and arrowheads, respectively) of Pattern II lesions. e and f: At higher magnification the Pattern II tissue appears vacuolated with a general reduction in the number of porin immunoreactive elements in EA (ee) and LA (eee) stages compared with NWM (e). f: The reduction in COX-I immunoreactive elements in EA (ff) and LA (fff) stage of Pattern II lesions is relative to the reduction of porin (e) elements. Scale bars = 40 μm (a), 8 mm (b–d) and 10 μm (e and f).

(complex IV activity) and succinate dehydrogenase (complex II activity). Since, frozen material from Pattern III multiple sclerosis lesions were not available we investigated hippocampal sections of a case with multiple mtDNA deletions. Since the extent of mitochondrial defects in primary mitochondrial disorders varies between cells in the nervous system, we found low expression of mtDNA encoded subunits (COX-I and complex I 20 kDa or ND6) in a subset of pyramidal cells of the CA2 layer, while nuclear DNA encoded proteins and the number of porin reactive mitochondria were unaffected (Fig. 6a–e). Quantitative studies on these cells, done by manual counting of immunoreactive mitochondria, revealed a 60% decrease in the number of COX-I reactive mitochondrial elements and show the feasibility and reliability of the manual counting method. This was confirmed by densitometry, showing a significant decrease ($P<0.001$) in COX-I reactivity within affected cells in comparison to unaffected adjacent cells.

In a snap frozen section of the contralateral hippocampus the enzyme histochemical analysis shows a proportion of cells, lacking complex IV activity with normal complex II activity (blue cells) and the remaining cells with complexes IV and II activity (brown cells; Fig. 6f). Cells deficient in COX-I and ND6 immunoreactivity or lacking complex IV activity were absent in similarly processed control tissue. These data indicate that the decrease in COX-I

Table 4 Quantitation of immunoreactive elements of mitochondrial respiratory chain subunits in WMS lesions

Mean ± SD (No. of lesions)	Porin	COX-I (mtDNA)	COX-IV (Nuclear)	Complex I 20 kDa or ND6 (mtDNA)	Complex I 30 kDa (Nuclear)	Complex II 70 kDa (Nuclear)
WMS	217.58 ± 17.67	186.64 ± 7.23	155.67 ± 14.59	133.62 ± 10.17	162.14 ± 10.58	124.13 ± 15.09
NWM	–	87 ± 9.2	73 ± 11.6	63 ± 10.1	73 ± 8.6	59 ± 13.9
(8–10)	133.8 ± 4.6	145.9 ± 3.7	159.0 ± 3.6	159.9 ± 4.5	153.3 ± 4.3	162.4 ± 4.6
WMS	182.41 ± 19.31*	93.96 ± 17.52†	113.44 ± 11.27	51.31 ± 12.65†	102.29 ± 14.51*	61.35 ± 9.30*
EA	–	49 ± 7.2†	63 ± 9.3	27 ± 7.7*	52 ± 10.5†	33 ± 10.1*
(7–9)	130.6 ± 4.8	173.1 ± 4.2*	159.2 ± 4.7	171.8 ± 4.9†	168.4 ± 3.9†	176.4 ± 4.8†

The values indicated in the first line are the mean and standard deviation of the absolute number of punctate elements per 100x field (6044 μm^2), second line are the mean and standard deviation of the percentages of porin elements containing respiratory chain complex subunit immunoreactivity (in serial sections) and third line are the mean and standard deviation of the densitometric values of whole grey scale 100x images. The densitometric value is inversely related to the intensity of the immunoreactivity. The number of lesions or NWM regions analysed for each stage is indicated within parentheses in column one. The immunoreactivity within lesions was compared with the corresponding NWM in multiple sclerosis and WMS cases ($^{\dagger}P < 0.01$ and $^{*}P < 0.001$).

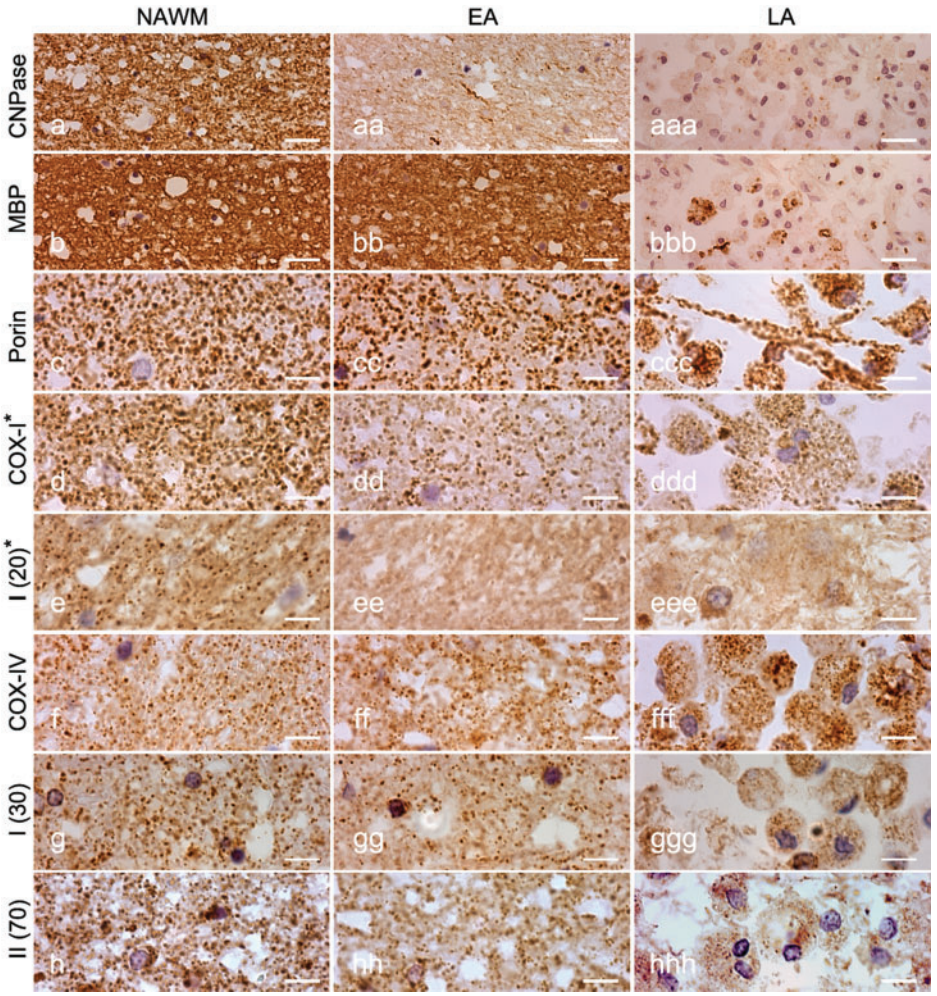

Fig. 5 WMS lesions. The three columns show immunoreactivity in NWM (left), EA (middle) and LA (right) stages of WMS tissue. a and b: Both CNPase and MBP immunoreactivity are detectable in the NWM, whereas CNPase immunoreactivity is lost while MBP immunoreactivity is intact in the EA stage of WMS lesions. In the LA stage, both CNPase and MBP immunoreactivity are lost except within phagocytic macrophages. c: The porin immunoreactive punctate elements are numerous in the NWM and EA stage. In the LA stage of WMS lesions, there is severe tissue loss and mitochondria are mostly located in phagocytic macrophages. d–h: The number of immunoreactive elements for all mitochondrial respiratory chain complex subunits (COX-I, complex I 20 kDa or ND6, complex I 30 kDa and complex II 70 kDa) except COX-IV appears decreased in EA stage compared with NWM. Furthermore, the majority of phagocytic macrophages in LA stage show a decrease in immunoreactivity for the mitochondrial respiratory chain complex subunits (except for COX-IV) despite the abundance of porin immunoreactive elements (ccc). Asterisk indicates subunits encoded by mtDNA. Scale bars = 10 μm (a–h).

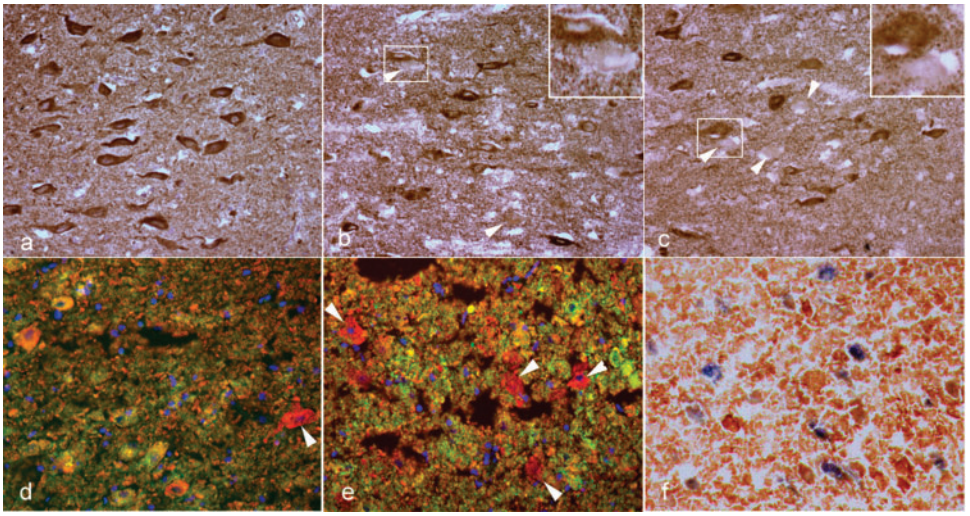

Fig. 6 The loss of mtDNA encoded respiratory chain subunit immunoreactivity in fixed brain tissue and implications for complex IV activity. (a–e) immunoreactivity in serial sections of fixed hippocampus. (f) activity of complexes II and IV in the snap frozen contralateral hippocampus. There are a number of cells containing complex II 70 kDa, a nuclear encoded subunit, immunoreactivity (a) in the CA2 layer of a fixed hippocampal section from a case with multiple deletions of mtDNA. In contrast, immunoreactivity for mtDNA encoded subunits [complex I 20 kDa or complex IV subunit I (COX-I)] is lacking in a proportion of cells, in serial sections (b and c, arrowheads and inserts). The cells lacking complex I 20 kDa or COX-I immunoreactivity (green) contain mitochondria (red) as shown by double immunofluorecent labelling with porin (d and e, arrowheads). The functional implications of the lack of COX-I immunoreactivity in fixed brain tissue can be clearly seen in a snap frozen section from the contralateral hippocampus where complex IV activity is lacking in a proportion of cells with complex II activity (f, blue).

immunoreactivity like that seen in Pattern III multiple sclerosis lesions is associated with a functional defect of the respiratory chain.

Discussion

In this study, we explored mitochondrial defects in fixed brain tissue from cases with multiple sclerosis by immunohistochemistry detecting a number of mtDNA and nuclear DNA encoded subunits of the respiratory chain complexes. We then directly compared the changes in acute multiple sclerosis lesions with those observed in WMS. In comparison to the white matter of normal brains and the NWM of multiple sclerosis tissue, we found two distinct patterns in mitochondrial changes. The first was reflected by a global reduction of mitochondrial density, seen also in sections stained for porin. This was seen in all multiple sclerosis and stroke tissues and apparently is due to the increase in extracellular space due to oedema and tissue loss/vacuolation. The second was a selective affection of certain mitochondrial proteins in relation to the global number of porin reactive mitochondria. This second pattern of mitochondrial alterations appears to be relevant for understanding mechanisms of tissue injury in the lesions.

In Pattern III lesions of multiple sclerosis patients, the mitochondrial proteins which were most affected, were COX-I and COX-IV. The analysis of the number of immunoreactive elements in serial sections shows that approximately a quarter of mitochondrial elements in EA and half of the mitochondrial elements in LA stages of Pattern III lesions lack COX-I immunoreactivity. It is well established that mtDNA encoded subunit-I of complex IV (COX-I) is essential for the activity of complex IV or COX (Comi *et al.*, 1998; Bruno *et al.*, 1999; Kollberg *et al.*, 2005). There was, however, also a deficiency of COX-IV (subunit IV of complex IV) in approximately a quarter of mitochondrial elements in Pattern III lesions. Although COX-IV is not a catalytic component of complex IV, it is important for the assembly of subunits as well as for the stability of complex IV (Nijtmans *et al.*, 1998; Taanman and Williams, 2001). A defect in COX-I leads to degradation of unassembled COX-IV, which may be the reason for a COX-IV defect in LA stage of Pattern III lesions (Nijtmans *et al.*, 1995). Alternatively, COX-IV may succumb to the same process that injures COX-I in Pattern III lesions. Hence, the mitochondrial defects in Pattern III lesions most likely impair activity, assembly and stability of complex IV. As shown in the case with multiple deletions of mtDNA and complex IV deficiency, the mitochondria devoid of COX-I immunoreactivity in Pattern III lesions are likely to lack complex IV activity.

The mitochondrial defects described above were seen in oligodendrocytes, axons and astrocytes, but not in macrophages and microglia. Oligodendrocytes are more susceptible to oxidative stress *in vitro* compared with astrocytes and microglia despite similar inhibition of mitochondrial activity (Mitrovic *et al.*, 1994). This differential susceptibility to oxidative stress may explain why oligodendrocytes undergo apoptosis in Pattern III lesions, while astrocytes are resistant. This difference may be due to astrocytes

being able to maintain ATP production through induction of glycolysis (Almeida *et al.*, 2001, 2004). Induction of glycolysis in astrocytes with mitochondrial defects causes an increase in lactate production (Almeida *et al.*, 2001). Indeed, magnetic resonance spectroscopic studies of Balo's type lesions have found consistently increased lactate peaks (Lindquist *et al.*, 2007; Mowry *et al.*, 2007). Furthermore, CSF lactate levels may be elevated in patients with primary mitochondrial disorders (Jackson *et al.*, 1995).

Mitochondrial injury may also be important in driving axonal degeneration. In acutely demyelinated axons, the efflux of sodium (Na^+) entering through the redistributed Na^+ channels and ionic homeostasis are energy dependant processes (Waxman, 2006). The demyelinated axons can be protected from NO mediated degeneration, which involves an energy deficient state, using Na^+ channel blockers or inhibitors of Na^+/Ca^{2+} exchanger (Garthwaite *et al.*, 2002; Kapoor *et al.*, 2003). Hence, the complex IV defect involving axons in Pattern III lesions may augment axonal degeneration through an increase in intra-axonal Na^+ and imbalance of Ca^{2+}.

What drives the complex IV defects in Pattern III lesions needs further investigation. The differential expression of mtDNA-encoded subunits is physiologically regulated at a post-transcriptional level. The COX-I mRNA is rapidly degraded *in vitro* compared to a number of other subunits when exposed to NO (Wei *et al.*, 2002). Hence, we speculate that the mitochondrial defects in Pattern III lesions identified in this study are due to post-transcriptional modification of COX-I mRNA by NO and subsequent degradation of unassembled COX-IV (Nijtmans *et al.*, 1995; Williams *et al.*, 2001; Wei *et al.*, 2002; Fukuda *et al.*, 2007). Alternative explanations include damage to COX-I gene (mutations of COX-I gene) or selective degradation of complex IV subunits. However, the above hypothesis does not address why the mitochondrial defects in acute lesions are confined to Pattern III in multiple sclerosis. There is evidence that distinct inflammatory pathways exist between Pattern II and Pattern III lesions. The expression of chemokine receptors differs in Pattern II from Pattern III lesions (Mahad *et al.*, 2004). The microglia appear to be activated via Toll-like receptors in the early stages of Pattern III and not Pattern II lesions (Smiley *et al.*, 2001; Marik *et al.*, 2007). These activated microglia, found in close proximity to apoptotic oligodendrocytes, may release a range of mediators (Barnett and Prineas, 2004; Perry *et al.*, 2007). Hence, the differences in immune response and extent of NO production may explain the selectivity of complex IV defects in acute multiple sclerosis lesions.

Little is known about the state of mitochondrial respiratory chain in WMS lesions. However, *in vitro* and *in vivo* studies have identified a decrease in transcription of mtDNA and nuclear DNA encoded subunits within 24 h of exposure to hypoxia (Vijayasarathy *et al.*, 2003; Piruat and Lopez-Barneo, 2005; Fukuda *et al.*, 2007). Accordingly, we identify a decrease in a number of immunohistochemically detectable subunits of complexes I, II and IV except COX-IV. What is intriguing about the profile of immunohistochemically detected mitochondrial respiratory chain subunits in WMS lesions is the preservation of COX-IV when COX-I is profoundly reduced (from 91% to 49%). COX-IV has two isoforms (COX-IV-1, which is present under physiological conditions and COX-IV-2). The stabilisation of HIF-1α by hypoxia increases transcription of COX-IV-2, which transfers electrons more efficiently than COX-IV-1 (Fukuda *et al.*, 2007). HIF-1α is up-regulated in WMS lesions and early stages of Pattern III lesions, where COX-IV is relatively preserved. HIF-1α is minimal or absent in LA stage of Pattern III lesions, where COX-IV is reduced (Marik *et al.*, 2007). The monoclonal antibody against COX-IV does not differentiate the isoforms. Hence, the stabilization of HIF-1α may explain the difference in immunohistochemically detected COX-IV between WMS and Pattern III lesions.

In conclusion, our study provides evidence for mitochondrial defects, which may at least in part explain the hypoxia-like tissue injury seen in a subtype of multiple sclerosis lesions. The data are consistent with the hypothesis that radicals, produced by activated macrophages and microglia, are a major driving force in the pathogenesis of such lesions. The mechanism of tissue injury, described here, may not be restricted to these fulminant lesions of acute and early relapsing multiple sclerosis. Microarray studies from cortical and white matter tissue of patients with progressive multiple sclerosis showed up-regulation of genes involved in (hypoxic) preconditioning (Graumann *et al.*, 2003) and decreased expression of mRNA for mitochondrial proteins (Dutta *et al.*, 2006). Furthermore, the dominant loss of small calibre axons in multiple sclerosis lesions suggests energy deficiency as a major mechanism involved in axonal degeneration (DeLuca *et al.*, 2004; Stys, 2005). Thus, the mitochondrial alterations seen in fulminant Pattern III multiple sclerosis lesions may in milder form also drive oligodendrocyte and axonal injury in the progressive stage of the disease.

Acknowledgements

This study was funded by the Welcome Trust and by the Austrian Science Fund (FWF, Project P 19854-B02). We thank the UK MS Tissue Bank for providing the control tissue, Dr T Booth for confocal microscopy, Prof. RN Lightowlers for guidance on mitochondrial subunit detection and Prof. RW Taylor for providing the case with multiple mtDNA deletions.

References

Aboul-Enein F, Rauschka H, Kornek B, Stadelmann C, Stefferl A, Bruck W, et al. Preferential loss of myelin-associated glycoprotein reflects hypoxia-like white matter damage in stroke and inflammatory brain diseases. J Neuropathol Exp Neurol 2003; 62: 25–33.

Almeida A, Almeida J, Bolanos JP, Moncada S. Different responses of astrocytes and neurons to nitric oxide: the role of glycolytically generated ATP in astrocyte protection. Proc Natl Acad Sci USA 2001; 98: 15294–9.

Almeida A, Moncada S, Bolanos JP. Nitric oxide switches on glycolysis through the AMP protein kinase and 6-phosphofructo-2-kinase pathway. Nat Cell Biol 2004; 6: 45–51.

Barnett MH, Prineas JW. Relapsing and remitting multiple sclerosis: pathology of the newly forming lesion. Ann Neurol 2004; 55: 458–68.

Bolanos JP, Almeida A, Stewart V, Peuchen S, Land JM, Clark JB, et al. Nitric oxide-mediated mitochondrial damage in the brain: mechanisms and implications for neurodegenerative diseases. J Neurochem 1997; 68: 2227–40.

Brown GC, Cooper CE. Nanomolar concentrations of nitric oxide reversibly inhibit synaptosomal respiration by competing with oxygen at cytochrome oxidase. FEBS Lett 1994; 356: 295–8.

Bruno C, Martinuzzi A, Tang Y, Andreu AL, Pallotti F, Bonilla E, et al. A stop-codon mutation in the human mtDNA cytochrome c oxidase I gene disrupts the functional structure of complex IV. Am J Hum Genet 1999; 65: 611–20.

Clark KM, Bindoff LA, Lightowlers RN, Andrews RM, Griffiths PG, Johnson MA, et al. Reversal of a mitochondrial DNA defect in human skeletal muscle. Nat Genet 1997; 16: 222–4.

Cleeter MW, Cooper JM, Darley-Usmar VM, Moncada S, Schapira AH. Reversible inhibition of cytochrome c oxidase, the terminal enzyme of the mitochondrial respiratory chain, by nitric oxide. Implications for neurodegenerative diseases. FEBS Lett 1994; 345: 50–4.

Clementi E, Brown GC, Feelisch M, Moncada S. Persistent inhibition of cell respiration by nitric oxide: crucial role of S-nitrosylation of mitochondrial complex I and protective action of glutathione. Proc Natl Acad Sci USA 1998; 95: 7631–6.

Comi GP, Bordoni A, Salani S, Franceschina L, Sciacco M, Prelle A, et al. Cytochrome c oxidase subunit I microdeletion in a patient with motor neuron disease. Ann Neurol 1998; 43: 110–6.

DeLuca GC, Ebers GC, Esiri MM. Axonal loss in multiple sclerosis: a pathological survey of the corticospinal and sensory tracts. Brain 2004; 127: 1009–18.

DiMauro S, Schon EA. Mitochondrial respiratory-chain diseases. N Engl J Med 2003; 348: 2656–68.

Dobersen MJ, Hammer JA, Noronha AB, MacIntosh TD, Trapp BD, Brady RO, et al. Generation and characterization of mouse monoclonal antibodies to the myelin-associated glycoprotein (MAG). Neurochem Res 1985; 10: 499–513.

Dutta R, McDonough J, Yin X, Peterson J, Chang A, Torres T, et al. Mitochondrial dysfunction as a cause of axonal degeneration in multiple sclerosis patients. Ann Neurol 2006; 59: 478–89.

Frohman EM, Racke MK, Raine CS. Multiple sclerosis–the plaque and its pathogenesis. N Engl J Med 2006; 354: 942–55.

Fukuda R, Zhang H, Kim JW, Shimoda L, Dang CV, Semenza GL. HIF-1 regulates cytochrome oxidase subunits to optimize efficiency of respiration in hypoxic cells. Cell 2007; 129: 111–22.

Garthwaite G, Goodwin DA, Batchelor AM, Leeming K, Garthwaite J. Nitric oxide toxicity in CNS white matter: an in vitro study using rat optic nerve. Neuroscience 2002; 109: 145–55.

Graumann U, Reynolds R, Steck AJ, Schaeren-Wiemers N. Molecular changes in normal appearing white matter in multiple sclerosis are characteristic of neuroprotective mechanisms against hypoxic insult. Brain Pathol 2003; 13: 554–73.

Itoyama Y, Sternberger NH, Webster HD, Quarles RH, Cohen SR, Richardson EP Jr. Immunocytochemical observations on the distribution of myelin-associated glycoprotein and myelin basic protein in multiple sclerosis lesions. Ann Neurol 1980; 7: 167–77.

Jackson MJ, Schaefer JA, Johnson MA, Morris AA, Turnbull DM, Bindoff LA. Presentation and clinical investigation of mitochondrial respiratory chain disease. A study of 51 patients. Brain 1995; 118 (Pt 2): 339–57.

Kalman B, Laitinen K, Komoly S. The involvement of mitochondria in the pathogenesis of multiple sclerosis. J Neuroimmunol 2007; 188: 1–12.

Kapoor R, Davies M, Blaker PA, Hall SM, Smith KJ. Blockers of sodium and calcium entry protect axons from nitric oxide-mediated degeneration. Ann Neurol 2003; 53: 174–80.

Kollberg G, Moslemi AR, Lindberg C, Holme E, Oldfors A. Mitochondrial myopathy and rhabdomyolysis associated with a novel nonsense mutation in the gene encoding cytochrome c oxidase subunit I. J Neuropathol Exp Neurol 2005; 64: 123–8.

Lassmann H, Bruck W, Lucchinetti C. Heterogeneity of multiple sclerosis pathogenesis: implications for diagnosis and therapy. Trends Mol Med 2001; 7: 115–21.

Lindquist S, Bodammer N, Kaufmann J, Konig F, Heinze HJ, Bruck W, et al. Histopathology and serial, multimodal magnetic resonance imaging in a multiple sclerosis variant. Mult Scler 2007; 13: 471–82.

Lucchinetti C, Bruck W, Parisi J, Scheithauer B, Rodriguez M, Lassmann H. Heterogeneity of multiple sclerosis lesions: implications for the pathogenesis of demyelination. Ann Neurol 2000; 47: 707–17.

Mahad DJ, Trebst C, Kivisakk P, Staugaitis SM, Tucky B, Wei T, et al. Expression of chemokine receptors CCR1 and CCR5 reflects differential activation of mononuclear phagocytes in pattern II and pattern III multiple sclerosis lesions. J Neuropathol Exp Neurol 2004; 63: 262–73.

Marik C, Felts PA, Bauer J, Lassmann H, Smith KJ. Lesion genesis in a subset of patients with multiple sclerosis: a role for innate immunity? Brain 2007; 130: 2800–15.

Mitrovic B, Ignarro LJ, Montestruque S, Smoll A, Merrill JE. Nitric oxide as a potential pathological mechanism in demyelination: its differential effects on primary glial cells in vitro. Neuroscience 1994; 61: 575–85.

Moncada S, Erusalimsky JD. Does nitric oxide modulate mitochondrial energy generation and apoptosis? Nat Rev Mol Cell Biol 2002; 3: 214–20.

Mowry EM, Woo JH, Ances BM. Balo's concentric sclerosis presenting as a stroke-like syndrome. Nat Clin Pract Neurol 2007; 3: 349–54.

Nijtmans LG, Spelbrink JN, Van Galen MJ, Zwaan M, Klement P, Van den Bogert C. Expression and fate of the nuclearly encoded subunits of cytochrome-c oxidase in cultured human cells depleted of mitochondrial gene products. Biochim Biophys Acta 1995; 1265: 117–26.

Nijtmans LG, Taanman JW, Muijsers AO, Speijer D, Van den Bogert C. Assembly of cytochrome-c oxidase in cultured human cells. Eur J Biochem 1998; 254: 389–94.

Perry VH, Cunningham C, Holmes C. Systemic infections and inflammation affect chronic neurodegeneration. Nat Rev Immunol 2007; 7: 161–7.

Piruat JI, Lopez-Barneo J. Oxygen tension regulates mitochondrial DNA-encoded complex I gene expression. J Biol Chem 2005; 280: 42676–84.

Rahman S, Lake BD, Taanman JW, Hanna MG, Cooper JM, Schapira AH, et al. Cytochrome oxidase immunohistochemistry: clues for genetic mechanisms. Brain 2000; 123 (Pt 3): 591–600.

Rizzuto R, Pozzan T. Microdomains of intracellular Ca2+: molecular determinants and functional consequences. Physiol Rev 2006; 86: 369–408.

Smiley ST, King JA, Hancock WW. Fibrinogen stimulates macrophage chemokine secretion through toll-like receptor 4. J Immunol 2001; 167: 2887–94.

Smith KJ, Lassmann H. The role of nitric oxide in multiple sclerosis. Lancet Neurol 2002; 1: 232–41.

Stadelmann C, Ludwin S, Tabira T, Guseo A, Lucchinetti CF, Leel-Ossy L, et al. Tissue preconditioning may explain concentric lesions in Balo's type of multiple sclerosis. Brain 2005; 128: 979–87.

Stys PK. General mechanisms of axonal damage and its prevention. J Neurol Sci 2005; 233: 3–13.

Taanman JW, Williams SL. Assembly of cytochrome c oxidase: what can we learn from patients with cytochrome c oxidase deficiency? Biochem Soc Trans 2001; 29: 446–51.

Taylor RW, Turnbull DM. Mitochondrial DNA mutations in human disease. Nat Rev Genet 2005; 6: 389–402.

Vijayasarathy C, Damle S, Prabu SK, Otto CM, Avadhani NG. Adaptive changes in the expression of nuclear and mitochondrial encoded subunits of cytochrome c oxidase and the catalytic activity during hypoxia. Eur J Biochem 2003; 270: 871–9.

Waxman SG. Axonal conduction and injury in multiple sclerosis: the role of sodium channels. Nat Rev Neurosci 2006; 7: 932–41.

Wei J, Guo H, Kuo PC. Endotoxin-stimulated nitric oxide production inhibits expression of cytochrome c oxidase in ANA-1 murine macrophages. J Immunol 2002; 168: 4721–7.

Williams SL, Scholte HR, Gray RG, Leonard JV, Schapira AH, Taanman JW. Immunological phenotyping of fibroblast cultures from patients with a mitochondrial respiratory chain deficit. Lab Invest 2001; 81: 1069–77.

Zhang J, Jin B, Li L, Block ER, Patel JM. Nitric oxide-induced persistent inhibition and nitrosylation of active site cysteine residues of mitochondrial cytochrome-c oxidase in lung endothelial cells. Am J Physiol Cell Physiol 2005; 288: C840–9.